



■ BONE BIOLOGY

Interleukin-19 promotes bone resorption by suppressing osteoprotegerin expression in BMSCs in a lipopolysaccharide-induced bone loss mouse model

**Z. Dai,
Y. Chen,
E. He,
H. Wang,
W. Guo,
Z. Wu,
K. Huang,
Q. Zhao**

From Shanghai General Hospital, Shanghai Jiao Tong University School of Medicine, Shanghai, China

Aims

Osteoporosis is characterized by decreased trabecular bone volume, and microarchitectural deterioration in the medullary cavity. *Interleukin-19 (IL-19)*, a member of the IL-10 family, is an anti-inflammatory cytokine produced primarily by macrophages. The aim of our study was to investigate the effect of *IL-19* on osteoporosis.

Methods

Blood and femoral bone marrow suspension *IL-19* levels were first measured in the lipopolysaccharide (LPS)-induced bone loss model. Small interfering RNA (siRNA) was applied to knock down *IL-19* for further validation. Thereafter, osteoclast production was stimulated with *IL-19* in combination with mouse macrophage colony-stimulating factor (M-CSF) and receptor activator of nuclear factor- κ B ligand (RANKL). The effect of *IL-19* was subsequently evaluated using tartrate-resistant acid phosphatase (TRAP) staining and quantitative real-time polymerase chain reaction (RT-qPCR). The effect of *IL-19* on osteoprotegerin (OPG) was then assessed using in vitro recombinant *IL-19* treatment of primary osteoblasts and MLO-Y4 osteoblast cell line. Finally, transient transfection experiments and chromatin immunoprecipitation (ChIP) experiments were used to examine the exact mechanism of action.

Results

In the LPS-induced bone loss mouse model, the levels of *IL-19* in peripheral blood serum and femoral bone marrow suspension were significantly increased. The in vivo results indicated that global *IL-19* deletion had no significant effect on RANKL content in the serum and bone marrow, but could increase the content of OPG in serum and femoral bone marrow, suggesting that *IL-19* inhibits OPG expression in bone marrow mesenchymal stem cells (BMSCs) and thus increases bone resorption.

Conclusion

IL-19 promotes bone resorption by suppressing OPG expression in BMSCs in a LPS-induced bone loss mouse model, which highlights the potential benefits and side effects of *IL-19* for future clinical applications.

Cite this article: *Bone Joint Res* 2023;12(11):691–701.

Keywords: Interleukin-19, Osteoprotegerin, Lipopolysaccharide, Bcl6

Article focus

- This study aimed to validate the lipopolysaccharide (LPS)-induced bone loss model.
- We explored the role of *interleukin-19 (IL-19)* in a model of LPS-induced bone loss.
- In doing so, we aimed to further improve the current understanding of the mechanisms of bone loss by inflammatory factors, and to orientate the targeting of *IL-19* for targeted regulation of bone loss-related diseases.

Correspondence should be sent to Qinghua Zhao; email: qinghua.zhao@shgh.cn

doi: 10.1302/2046-3758.1211.BJR-2023-0101.R1

Bone Joint Res 2023;12(11):691–701.

Key messages

- *IL-19* promotes bone resorption via suppressing osteoprotegerin (OPG) expression in bone mesenchymal stem cells (BMSCs) in a LPS-induced bone loss mouse model.
- *IL-19* suppresses OPG expression via Bcl6 in BMSCs.

Strengths and limitations

- For the first time, this study revealed that *IL-19* promotes bone resorption by inhibiting OPG.
- Further investigations regarding the detailed molecular mechanisms are required.

Introduction

Osteoporosis is a common skeletal disease characterized by altered bone metabolism, microarchitectural deterioration, decreased bone mass, and increased fragility fracture risk.^{1,2} Bone metabolic homeostasis requires a delicate balance between osteoblast-mediated bone formation and osteoclast-mediated bone resorption. The disruption of this balance underlies the pathogenesis of osteoporosis.³ Clinically, bone loss is a common complication in patients with inflammatory conditions, and severe bone loss due to excessive bone resorption by osteoclasts is observed in inflammatory osteolytic diseases, such as osteomyelitis, septic arthritis, infection of orthopaedic implants, and traumatic bacterial infection.^{1,2} The infiltration of inflammatory mediators into the inflamed region helps to increase osteoclast differentiation and activity, thus increasing bone resorption.⁴⁻⁶ As a key pathogen, lipopolysaccharide (LPS), a major constituent of Gram-negative bacteria, can induce bone loss, leading to increased fragility fracture risk.³ It has been shown that LPS-induced tumour necrosis factor- α (TNF- α) secretion regulates osteoclast differentiation independently by possibly activating TNFR-2, which is consistent with the mechanism of action of Gram-positive cocci *Staphylococcus aureus* targeting osteoblasts.⁷⁻⁹ LPS-induced excessive osteoclast differentiation is the main cause of bone loss. Osteoclasts are multinucleated bone-resorbing cells that differentiate from bone marrow monocytes (BMMs), in the presence of two indispensable cytokines: macrophage colony-stimulating factor (M-CSF) and receptor activator of nuclear factor (NF)- κ B ligand (RANKL).^{10,11} LPS induces the production of pro-inflammatory cytokines such as TNF- α , interleukin-1 β (IL-1 β), IL-6, and prostaglandin E2 (PGE2) to directly stimulate osteoclastogenesis by increasing the expression of RANKL.³ It has been shown that RANKL inhibits the decrease of Connexin 43 protein during osteoclast-induced differentiation, while LPS promotes the expression of receptor activator of NF- κ B (RANK) protein, suggesting that LPS may promote osteoclast proliferation and differentiation by interacting with Connexin 43 protein molecules through the RANKL/RANK/osteoprotegerin (OPG) signalling pathway.¹² LPS affects not only osteoclasts but also osteoblasts. The action of LPS on osteoblasts causes them to release RANK, and Toll-like receptor 4 (TLR4) binds to RANK, causing

NF- κ B to be upregulated and thus regulating the activity of osteoblasts.¹³ Effective therapies against LPS-induced bone loss models that are not models of osteoporosis are limited to antibiotics and surgery. It is important to elucidate the mechanisms of bone destruction induced by LPS to find new strategies to treat inflammatory osteolytic diseases.

IL-19 is primarily produced by various immune cells, keratinocytes, fibroblasts, and epithelial cells.¹⁴ As a member of the IL-10 family of cytokines, *IL-19* mediates its function by binding to the *IL-20* receptor complex.^{14,15} Studies have highlighted the important role of *IL-19* in immunological and inflammatory diseases.¹⁵⁻¹⁸ Increased plasma concentration of *IL-19* is associated with the pathogenesis of both helper T cell 1 (Th1) and helper T cell 2 (Th2) dominant diseases, such as psoriasis and asthma. In addition, studies have shown that its expression can be induced by LPS.¹⁷ *IL-19* is upregulated in macrophages after infection and lessens inflammation by suppressing the production of TNF- α , IL-6, and IL-12. *IL-19* is a potential therapeutic in immunological and inflammatory diseases.^{16,17} However, the contribution of *IL-19* in LPS-induced bone loss is largely unknown.

The RANKL/OPG axis is critical for regulating bone resorption. RANKL is expressed largely in bone, and bone mesenchymal stem cells (BMSCs), osteoblasts, and osteocytes are major sources of RANKL for osteoclastogenesis.¹⁹⁻²¹ RANKL was required to induce osteoclast formation in the presence of M-CSF. OPG was identified as a secreted glycoprotein synthesized by several kinds of cells including BMSCs, osteoblasts, osteocytes, B lymphocytes, and articular chondrocytes.^{20,21} Additionally, studies have revealed that OPG could inhibit osteoclast differentiation as a soluble decoy receptor of RANKL to antagonize the effects of RANKL.¹⁹⁻²¹ BMSCs can modulate osteoclastogenesis by producing RANKL and OPG.²⁰ Therefore, preventing osteoclast activation, especially regulating the RANKL/OPG axis, is one effective way to treat LPS-induced bone loss in clinics.

In this study, we investigated the effects of *IL-19* on the skeletal system in a mouse model of LPS-induced bone loss, to reveal its potential benefits and side effects for future clinical applications.

Methods

Animals. A total of 48, ten-week-old male C57BL/6 mice were housed in a specific pathogen-free (SPF) environment, and all mice were provided with sterile food and water. Since female mice undergo changes with the growth and development of oestrogen in the body, and there is a state of oestrogen mutation, and oestrogen has been proven to have a correlation with osteoporosis, which may interfere with the experimental results, male mice were selected for the experiments. We determined the experimental sample size ($n = 8$) based on previous experience and literature. After that, we used the experimental LPS induction model data and *IL-19* level data to calculate the minimum sample size ($n = 6$) using PASS

2021 software (Number Cruncher Statistical System (NCSS), USA) under the two-sided condition of power calculation of 0.9 ($\beta = 0.1$) and α of 0.05. Considering the uncertainty of the experiment and the possibility of animal failure and death, we chose $n = 8$ as the experimental sample size. The animal experiments were performed in accordance with the approved guidelines by the Institutional Animal Care and Use Committee affiliated with Shanghai General Hospital, Shanghai Jiao Tong University School of Medicine. Animal experiments were conducted according to the 3Rs and adhered to the ARRIVE guidelines; an ARRIVE checklist is included in the Supplementary Material.

LPS-induced bone loss mouse model. Male C57BL/6 mice were intraperitoneally (i.p.) treated with 5 mg/kg LPS. 'Day 0' was defined as the first time when LPS was administered, and the second time when LPS was administered is referred to as 'Day 3'. The mice i.p. treated with phosphate-buffered saline (PBS) were used as negative controls. Peripheral blood was harvested on Days 0, 3, 6, and 9. Lumbar (L) #1 vertebrae and femora were collected on Day 9. Due to the very small calibre of the murine tail veins, i.p. injection of LPS/PBS was used for our experiments.

IL-19 knockout mouse model. F1 embryonic stem cells that carried the *IL-19*-deficient construct were injected into C57BL/6 blastocytes. The derived heterozygous mice were backcrossed onto the C57BL/6 genetic background for at least 12 generations. Mice with and without *IL-19* were inter-crossed to generate mutant and control mice. *IL-19*^{-/-} mice were identified by genotyping of tail DNA by polymerase chain reaction (PCR) using specific primer.

Cell cultures. Primary BMMs were isolated from mice. Briefly, the bone marrow cells were flushed out from femur and tibia bones with α -Minimum Essential Medium (MEM) (HyClone; Danaher Corporation, USA). Cell suspensions were filtered through a 100 μ m cell strainer (Falcon; Corning, USA) and cultured in α -MEM supplemented with 10% fetal bovine serum (FBS) (MilliporeSigma, USA), 1% penicillin/streptomycin (Invitrogen; Thermo Fisher Scientific, USA), and 1% GlutaMAX Supplement (Thermo Fisher Scientific) for 24 hours. The supernatant was collected and cell precipitation was obtained by centrifugation, then BMMs were cultured in α -MEM medium supplemented with 10% FBS, 1% GlutaMAX Supplement, and 30 ng/ml M-CSF (PeproTech, Thermo Fisher Scientific) in a humidified atmosphere at 37°C and 5% CO₂. BMMs were harvested at Day 2 after M-CSF stimuli. For osteoclast differentiation, harvested BMMs were seeded into 12-well plates at a concentration of 1×10^5 cells per well for differentiation experiments. Cells were stimulated with 50 ng/ml RANKL (462-TEC-010; R&D Systems, USA) and 30 ng/ml M-CSF (315-02-50; PeproTech) for seven days, and the medium was replaced every two days. Osteoclasts were fixed and stained using the tartrate-resistant acid phosphatase (TRAP) staining kit

Table 1. Primer sequences used for real-time polymerase chain reaction.

Gene	Primer sequence (5'-3')	Product length, bp
OPG	CCTAAAGCGTTAACCCCGGA (F)	120
	AACAGGAAGTATGCCCTGCC (R)	
Cathepsin K	CTGCGGCATTACCAACATGG (F)	192
	ACTGGAAGCACCAACGAGAG (R)	
β 3-integrin	GGACAACCTCTGGGCCGCTC (F)	181
	CCTTCAGGTTACATCGGGGTG (R)	
DC-STAMP	CCGTGAAGGTAGGAACGCTT (F)	207
	AGATTCAGCGGAGTGGCAAG (R)	
ATP6v0d2	GGCCAGTGTTCAAGTTGCTA (F)	213
	AGTCCGTGGTCTGGAGATGA (R)	
α -tubulin	TGTGGATTCTGTGGAAGGCG (F)	149
	AGCACACATTGCCACATACAAA (R)	

F, forward; OPG, osteoprotegerin; R, reverse.

(387A-1KT; MilliporeSigma). TRAP+ cells with more than three nuclei were considered as mature osteoclasts. TRAP+ cells with more than five nuclei were considered as large osteoclasts.

Briefly, femur and tibia bones were obtained and rinsed while stripping muscle tissue, and then soft-tissue was removed and transferred to the culture medium. The bone tissue was minced with forceps and washed with a 1 ml syringe to obtain bone marrow cells, which were seeded and cultured. After two days, the medium was changed and sub-cultured. Cells at passage 6 were used for cell function experiments.

Primary osteocytes were isolated from mice. Briefly, long bones were obtained and processed for digestion with α -MEM medium containing 300 U/ml collagenase type Ia (MilliporeSigma). The digestion step was performed in six-well dishes on a rotary shaker set to 200 rpm in a humidified incubator at 37°C and 5% CO₂. After digestion, the solution was removed from the bone fragments and stored. The bone fragments were rinsed with Hank's Balanced Salt Solution (HBSS), then added to the digestive fluid. The cell suspension was centrifuged at 200 g for five minutes, the supernatant removed, and the cells resuspended in medium. Cell suspensions from the primary isolation procedure were grown on type I collagen-coated six-well plates. Cells were maintained for seven days in a humidified incubator at 37°C and 5% CO₂.

Mouse osteocyte cell lines (MLO-Y4) were obtained from American Type Culture Collection (ATCC, USA). They were cultured in DMEM with 10% FBS (MilliporeSigma) and incubated in a humidified atmosphere at 37°C and 5% CO₂.

Randomization. A total of 48 mice were randomly divided into six groups of eight mice each (Supplementary Table i). All animals were divided into four different body weight groups (12 animals per group). One cage was randomly selected from all cages (12 in total), and one animal from each body weight range group was placed in the cage separately. This was repeated until all animals

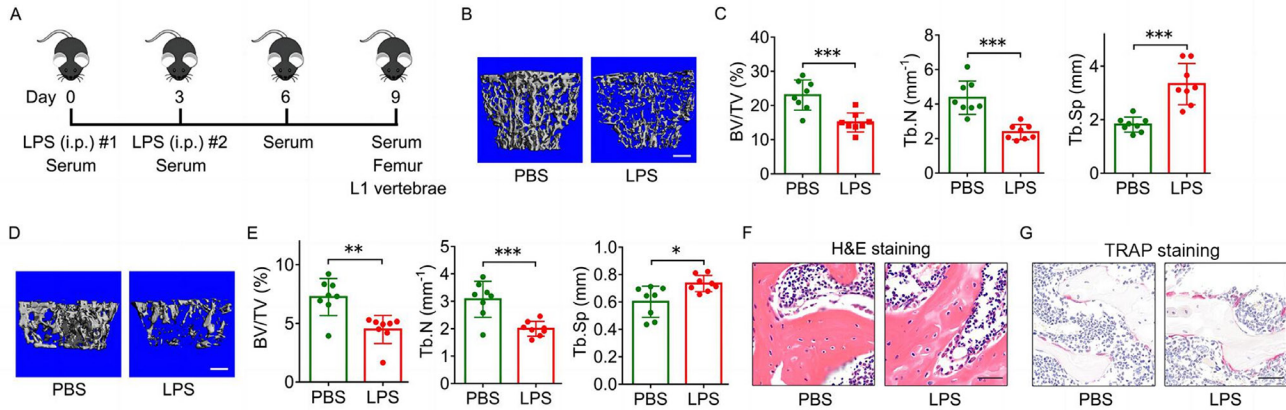


Fig. 1

Lipopolysaccharide (LPS)-induced trabecular bone loss and bone resorption improvement in mice. a) Schematic diagram of mice intraperitoneally (i.p.) treated with 5 mg/kg LPS. The mice i.p. treated with phosphate-buffered saline (PBS) were used as negative controls. The day when LPS was administered for the first time was referred to as 'Day 0'. Second LPS was administered on Day 3. Peripheral blood serum was harvested on Days 0, 3, 6, and 9. Lumbar (L) #1 vertebrae and femora were collected on Day 9. b) Representative 3D reconstruction images of L1 vertebrae trabecular bone in LPS-induced bone loss of mice, determined by micro-CT. Scale bar: 400 μm . c) Trabecular bone volume fraction (BV/TV), trabecular number (Tb.N), and trabecular separation (Tb.Sp) of L1 vertebrae in LPS-induced bone loss of mice ($n = 8$). d) Representative 3D reconstruction images of distal femur trabecular bone in LPS-induced bone loss of mice, determined by micro-CT. Scale bar: 400 μm . e) BV/TV, Tb.N, and Tb.Sp of distal femur in LPS-induced bone loss of mice ($n = 8$). f) Haematoxylin and eosin (H&E) staining of femur trabecular bone in LPS-induced bone loss of mice ($n = 8$). Scale bar: 40 μm . g) Tartrate-resistant acid phosphatase (TRAP) staining of femur bone in LPS-induced bone loss of mice ($n = 8$). Scale bar: 40 μm . Data are representative of three independent experiments, and values are shown as means and standard deviations. P-values were determined by independent-samples *t*-test (c, e). * $p < 0.05$, ** $p < 0.01$, *** $p < 0.001$.

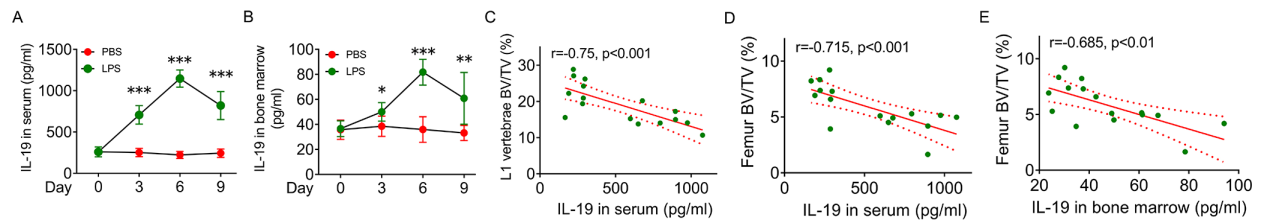


Fig. 2

The involvement of *interleukin (IL)-19* accumulation in serum and bone marrow in trabecular bone loss. a) *IL-19* levels in peripheral blood serum in lipopolysaccharide (LPS)-induced bone loss of mice on Day 0, 3, 6, and 9, determined by enzyme-linked immunosorbent assay (ELISA) ($n = 8$). b) *IL-19* levels in femur bone marrow aspirates in LPS-induced bone loss of mice on Day 0, 3, 6, and 9, determined by ELISA ($n = 8$). c) and d) The correlation of *IL-19* levels in serum with bone volume fraction (BV/TV) of c) L1 vertebrae and d) femur. e) The correlation of *IL-19* levels in bone marrow aspirates with BV/TV of femur. Data are representative of three independent experiments. Data are shown as means and standard deviations. P-values were determined by two-way analysis of variance (ANOVA) followed by Tukey's test (a, b) and Spearman correlation analyses (c, d, e). * $p < 0.05$, ** $p < 0.01$, *** $p < 0.001$.

were separated into cages. Each cage was given a number that randomized the position of the cages, and the numbers were randomly grouped into six groups. The random grouping was performed using a computer-based random order generator (Visual Studio; Microsoft, USA).

Blinding/masking. For each animal, three different operators (ZD, YC, WG) were involved as follows: the first operator administered the treatment according to a randomization table (this operator was the only one who knew the grouping); the second operator was responsible for the experimental manipulation; and the third operator performed the data recording. Finally, data analysis was performed jointly by the second and third operators.

Micro-CT analysis. Quantitative tomography of L1 vertebrae and distal femora was performed using an X-ray micro-CT (Skyscan 1076; Bruker, Belgium). The standardized regions of femur were scanned at 9 μm resolutions. Trabecular bone

mass and microarchitecture were defined, including trabecular bone volume fraction (BV/TV), trabecular number (Tb.N), and trabecular separation (Tb.Sp).

ELISA. The blood collected from mice was centrifuged for 30 minutes at 2,000 $\times g$, and the serum was harvested and stored at -80°C for subsequent assays. *IL-19*, RANKL, and OPG concentrations in the serum were all measured according to the manufacturer's instructions. The kits used in our enzyme-linked immunosorbent assay (ELISA) method were *IL-19* ELISA kits (NBP3-06800; Novus Biologicals; Bio-Techne, USA), RANKL ELISA kits (MTR00; R&D Systems), and OPG ELISA kits (MOP00; R&D Systems).

Bone histomorphometry analysis. After 4% formaldehyde fixation, decalcification with 10% EDTA (pH 7.4) for one week, and paraffin-embedded (formalin-fixed, paraffin-embedded (FFPE)) specimen processing,²² bone sections (5 to 7 μm) were stained with haematoxylin and eosin

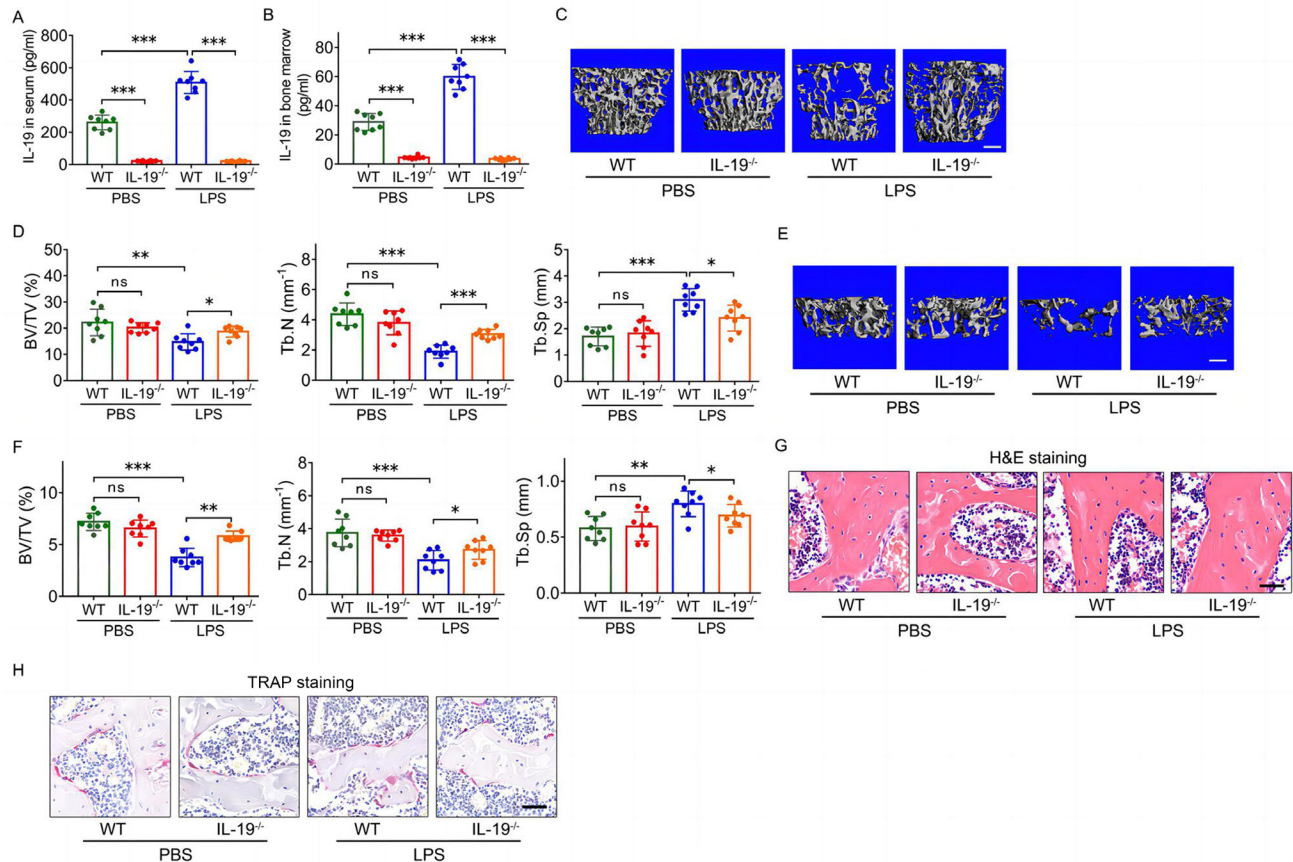


Fig. 3

Global deletion of *interleukin (IL)-19* counteracts lipopolysaccharide (LPS)-induced trabecular bone loss and bone resorption improvement in mice. a) and b) *IL-19* levels in a) peripheral blood serum and b) bone marrow aspirates in LPS-induced bone loss of *IL-19*^{-/-} mice, determined by enzyme-linked immunosorbent assay (ELISA) (n = 8). c) Representative 3D reconstruction images of lumbar (L) #1 vertebrae trabecular bone in LPS-induced bone loss of *IL-19*^{-/-} mice, determined by micro-CT. Scale bar: 400 μ m. d) Bone volume fraction (BV/TV), trabecular number (Tb.N), and trabecular separation (Tb.Sp) of L1 vertebrae in LPS-induced bone loss of mice (n = 8). e) Representative 3D reconstruction images of distal femur trabecular bone in LPS-induced bone loss of *IL-19*^{-/-} mice, determined by micro-CT. Scale bar = 400 μ m. f) BV/TV, Tb.N, and Tb.Sp of distal femur in LPS-induced bone loss of *IL-19*^{-/-} mice (n = 8). g) Haematoxylin and eosin (H&E) staining of femur trabecular bone in LPS-induced bone loss of mice (n = 8). Scale bar: 40 μ m. h) Tartrate-resistant acid phosphatase (TRAP) staining of femur bone in LPS-induced bone loss of mice (n = 8). Scale bar: 40 μ m. Data are representative of three independent experiments, and shown as means and standard deviations. P-values were determined by one-way analysis of variance (ANOVA) followed by Tukey's test (a, b, d, f). *p < 0.05, **p < 0.01, ***p < 0.001. ns, no significance; PBS, phosphate-buffered saline; WT, wild-type.

(H&E) and TRAP for histological evaluation of osteoblasts and osteoclasts in mice.

Western blot analysis. Cells were lysed in sodium dodecyl sulphate (SDS)-lysis buffer. The protein samples were loaded into the SDS polyacrylamide gel electrophoresis (SDS-PAGE) gels and then transferred onto nitrocellulose membranes (Axygen, USA). Membranes were blocked with 5% skimmed milk at room temperature for one hour and incubated with primary antibodies at 4°C overnight, following by incubation with horseradish peroxidase (HRP)-conjugated secondary antibodies at room temperature for one hour. Finally, the membranes were visualized with an Enhanced Chemiluminescence (ECL) Detection Kit (MilliporeSigma, USA) and by using ImageQuant LAS 4000 Mini (GE Healthcare Bio-Sciences AB, Sweden). The western blot used was 12% SDS-PAGE with a loading volume of 10 μ g per well, and the antibody stock numbers were as follows: IL-20R1: PA5-87796 (Thermo Fisher Scientific);

α -tubulin: #2125 (Cell Signaling Technology, USA); and Bcl-6: #5650 (Cell Signaling Technology).

Quantitative RT-PCR. Total RNA was extracted from cells by Trizol reagent (Invitrogen) and was reverse-transcribed into complementary DNA (cDNA) with AMV Reverse Transcriptase XL (Takara, Japan). Quantitative real-time PCR was performed using SYBR Green PCR Master Mix (Applied Biosystems; Thermo Fisher Scientific, USA) and on the ABI 7300 PCR system (Applied Biosystems). The reaction system was as follows: 4.5 μ l double-distilled water (ddH₂O) + 0.1 μ l 20 mM positive primer + 0.1 μ l 20 mM antisense primer + 0.1 μ l cDNA + 0.2 μ l RoxII + 5 μ l SYBR Premix. The procedure of real-time PCR were as follows: 40 cycles at 94°C for ten seconds, 60°C for 30 seconds. Dissociation stage was added to the end of the amplification procedure. There is no non-specific amplification determined by dissolve curve. α -tubulin was used as reference gene. The primer crossed

the intron/exon boundary. The primer sequences used are shown in Table I.

RNAi. Small interfering RNAs (siRNAs) were purchased from GeneCopoeia (USA). After cells were grown up to 40% to 60% confluence in α -MEM, the appropriate siRNAs were transfected into cells using Lipofectamine 3000 (Invitrogen), according to the manufacturer's instructions. After 24 hours, western blot was conducted to evaluate the silencing effect of the siRNA on target gene expression.

Luciferase reporter assay. Cells were cultured in 24-well plates. All plasmids were prepared using QIAGEN plasmid purification kit (Qiagen, Germany). Transient transfection was performed using Lipofectamine 3000 (Invitrogen) and phRL-SV40 vector (Promega, USA) was used as transfection efficiency control. Then, 48 hours after transfection, the cells were lysed, and both firefly and renilla luciferase activities were evaluated using Dual-Luciferase Reporter Assay System (Promega).

Chromatin immunoprecipitation. Enrichment of Bcl6 and RNA polymerase II (RNAP II) on the OPG promoter region was predicted using Cistrome Data Browser developed by Tongji University, China. Chromatin immunoprecipitation (ChIP) analysis was performed using the Millipore ChIP Assay Kit (MilliporeSigma) according to the manufacturer's instructions. Briefly, ChIP was performed with 5×10^6 cells per reaction. Cells were crosslinked with formaldehyde for ten minutes at room temperature and then sonicated. Isotype immunoglobulin G (IgG) was used as a control. The primer sequences used were 5'-TTTCTTCTTCTTCCCCCT-3' (F) and 5'-GCTAGGTGCGTCTCTGCAGC-3' (R), with a product length of 270 bp.

Statistical analysis. SPSS v21.0 (IBM, USA) was used to perform the statistical analysis. Independent-samples *t*-test was used for two-sample comparisons. One-way analysis of variance (ANOVA) and two-way ANOVA were used for multiple comparisons, and Tukey's test was used to find significant differences in ANOVA. Spearman correlation analyses were also applied in this study to investigate the correlation between variables. Statistical significance was set at $p < 0.05$. All data are presented as means and standard deviations unless otherwise specified.

Results

LPS-induced trabecular bone loss and bone resorption improvement in mice. To investigate inflammatory bone loss in vivo, we generated a LPS-induced trabecular bone loss mouse model (Figure 1a). The micro-CT analysis of L1 vertebrae and distal femur showed that the mice i.p. treated with LPS exhibited markedly reduced bone mass (Figures 1b and 1d), characterized with decreased BV/TV, trabecular bone number (Tb.N), bone surface/bone volume (BS/BV), and bone mineral density (BMD), and increased trabecular separation (Tb.Sp) (Figures 1c and 1e, Supplementary Figures aa and ab, Supplementary Table ii). These results suggest that LPS significantly promotes bone loss in mice. To examine whether LPS disrupted the dynamic balance between bone formation

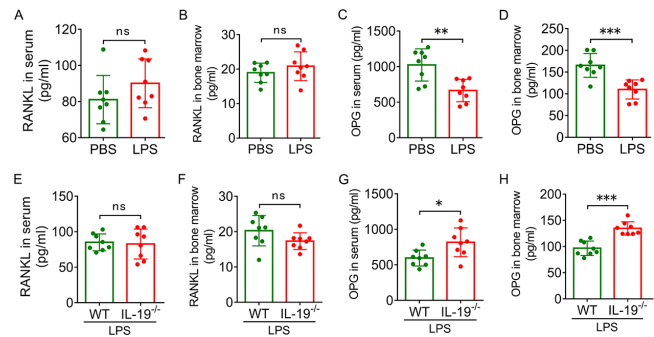


Fig. 4

Interleukin (IL)-19 suppresses osteoprotegerin (OPG) production in lipopolysaccharide (LPS)-induced bone loss of mice. Receptor activator of nuclear factor- κ B ligand (RANKL) levels in a) peripheral blood serum and b) bone marrow aspirates in LPS-induced bone loss of mice, determined by enzyme-linked immunosorbent assay (ELISA) ($n = 8$). OPG levels in c) peripheral blood serum and d) bone marrow aspirates in LPS-induced bone loss of mice, determined by ELISA ($n = 8$). RANKL levels in e) peripheral blood serum and f) bone marrow aspirates in LPS-induced bone loss of *IL-19*^{-/-} mice, determined by ELISA ($n = 8$). OPG levels in g) peripheral blood serum and h) bone marrow aspirates in LPS-induced bone loss of *IL-19*^{-/-} mice, determined by ELISA ($n = 8$). Data are representative of three independent experiments, and shown as means and standard deviations. P-values were determined by independent-samples *t*-test (c, d, g, h). * $p < 0.05$, ** $p < 0.01$, *** $p < 0.001$. ns, no significance.

and resorption, we measured the number of osteoblasts and osteoclasts on the surface of femur trabecular bone. There were no differences in the number of osteoblasts on the relative bone surface (Ob.N/B.Pm) and the percentage of bone surface occupied by osteoblasts (Ob.S/BS) between LPS- and PBS-treated mice (Figure 1f). However, the number of osteoclasts on the relative bone surface (Oc.N/B.Pm) and the percentage of bone surface occupied by osteoclasts (Oc.S/BS) were increased significantly in LPS-treated mice compared with PBS-treated mice (Figure 1g), suggesting an enhancement of bone resorption in LPS-treated mice.

IL-19 accumulation in serum and bone marrow in mice with LPS-induced trabecular bone loss. In the LPS-induced bone loss mouse model, the levels of *IL-19* in peripheral blood serum (Figure 2a) and femoral bone marrow suspension (Figure 2b) were significantly increased (Supplementary Table iii). Correlation analysis confirmed that the level of *IL-19* in serum was negatively correlated with BV/TV of L1 vertebrae (Figure 2c) and distal femur (Figure 2d) trabecular bone. *IL-19* content in the bone marrow suspension was also negatively correlated with BV/TV of distal femur trabecular bone in mice (Figure 2e).

Global deletion of IL-19 counteracts LPS-induced trabecular bone loss and bone resorption improvement. Since *IL-19* is involved in LPS-induced bone loss in mice, we generated the *IL-19* knockout (*IL-19*^{-/-}) mice. In *IL-19*^{-/-} mice, the volume of *IL-19* in peripheral blood (Figure 3a) and femoral bone marrow cavity (Figure 3b) was significantly decreased, regardless of whether LPS treatment was applied or not (Supplementary Table iv). WT and *IL-19*^{-/-} mice were treated with LPS or PBS. As revealed by micro-CT analysis of L1 vertebrae (Figure 3c)

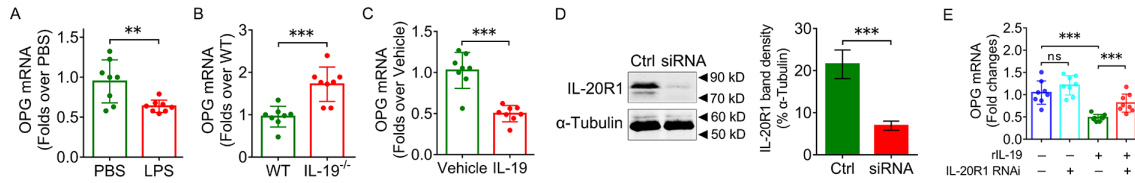


Fig. 5

Interleukin (IL)-19 suppresses osteoprotegerin (OPG) expression in bone mesenchymal stem cells (BMSCs). a) OPG messenger RNA (mRNA) expression of BMSCs in lipopolysaccharide (LPS)-induced bone loss of mice, determined by quantitative real-time polymerase chain reaction (RT-qPCR) (n = 8). b) OPG mRNA expression of BMSCs in LPS-induced bone loss of *IL-19*^{-/-} mice, determined by RT-qPCR (n = 8). c) OPG mRNA expression in in vitro primary BMSCs culture in response to 100 ng/ml recombinant *IL-19* treatment for 48 hours, determined by RT-qPCR (n = 8). d) Lentivirus-mediated stable knockdown of *IL-20R1* in in vitro BMSCs culture, determined by western blot. e) OPG mRNA expression in in vitro primary BMSCs culture in response to *IL-20R1* knockdown and/or 100 ng/ml recombinant *IL-19* treatment for 48 hours, determined by RT-qPCR and western blot. Data are representative of three independent experiments, and shown as means and standard deviations. P-values were determined by independent-samples *t*-test (a, b, c, d) and one-way analysis of variance (ANOVA) followed by Tukey's test (e). ***p* < 0.01, ****p* < 0.001. Ctrl, control; ns, no significance; *rIL-19*, recombinant *IL-19*; RNAi, RNA interference; siRNA, small interfering RNA; WT, wild-type.

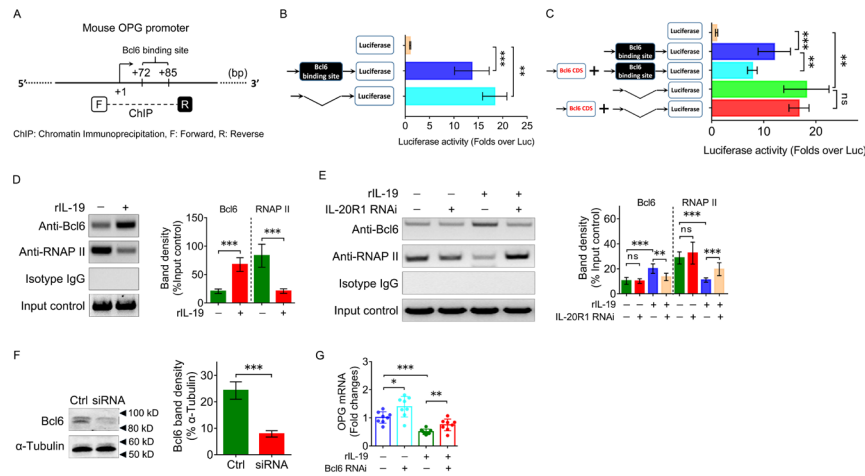


Figure 6

Fig. 6

Interleukin (IL)-19 suppresses osteoprotegerin (OPG) expression via Bcl6 in bone mesenchymal stem cells (BMSCs). a) Diagram of mouse OPG proximal promoter. Analysis of transcription factor binding sites in OPG promoter revealed a Bcl6 binding site close to the transcription start site. b) Luciferase activity of OPG promoter deletion mutant-driven luciferase reporter gene vectors, including Luc (empty vector as negative control), OPG promoter containing putative Bcl6 binding site, and OPG promoter with deletion of putative Bcl6 binding site in BMSCs when treated with 100 ng/ml recombinant *IL-19* for 48 hours (n = 8). c) Luciferase activity of OPG promoter deletion mutant-driven luciferase reporter gene vectors with or without pcDNA3.1-Bcl6 vector co-transfection in BMSCs when treated with recombinant *IL-19* for 48 hours (n = 8). d) Bcl6 and RNA polymerase II (RNAP II) binding on OPG promoter in BMSCs in response to 100 ng/ml recombinant *IL-19* treatment for 24 hours, determined by chromatin immunoprecipitation (ChIP). e) Bcl6 and RNAP II binding on OPG promoter in BMSCs in response to *IL-20R1* knockdown and/or 100 ng/ml recombinant *IL-19* treatment for 24 hours, determined by ChIP. f) Lentivirus-mediated stable knockdown of Bcl6 in in vitro BMSC culture, determined by western blot. g) OPG messenger RNA (mRNA) expression in in vitro primary BMSC culture in response to Bcl6 knockdown and/or 100 ng/ml recombinant *IL-19* treatment for 48 hours, determined by quantitative real-time polymerase chain reaction (RT-qPCR) (n = 8). Renilla luciferase vector was used as control for transfection efficiency. Isotype immunoglobulin G (IgG) was used as negative control in ChIP assay. α -tubulin was used as loading control in RT-qPCR and western blot. Data are representative of three independent experiments, and shown as means and standard deviations. P-values were determined by independent-samples *t*-test (d, f) and one-way analysis of variance (ANOVA) followed by Tukey's test (b, c, e, g). **p* < 0.05, ***p* < 0.01, ****p* < 0.001. Ctrl, control; F, forward; ns, no significance; R, reverse; *rIL-19*, recombinant *IL-19*; RNAi, RNA interference; siRNA, small interfering RNA.

and distal femur (Figure 3e), global *IL-19* deletion prevented LPS-induced trabecular bone loss, characterized by increased BV/TV, Tb.N, BS/BV, and BMD, and decreased Tb.Sp (Figures 3d and 3f, Supplementary Figures ac and ad, Supplementary Table v). Moreover, global *IL-19* deletion had no effect on bone formation (Figure 3g), but suppressed osteoclastogenesis (Figure 3h) in the LPS-treated mice group. ***IL-19* suppresses OPG expression in BMSCs.** To further verify whether *IL-19* directly regulates osteoclast differentiation,

BMMs were isolated from mice and treated with *IL-19* combined with murine M-CSF and RANKL stimulation to generate osteoclasts. TRAP staining showed that *IL-19* had no obvious effect on osteoclast differentiation, as characterized by the similar number of TRAP-positive osteoclasts (Supplementary Figure ba). Consistently, the expression of osteoclastogenesis marker genes Cathepsin K, β 3-integrin, DC-STAMP, and ATP6v0d2 remained unchanged between the groups with and without *IL-19*

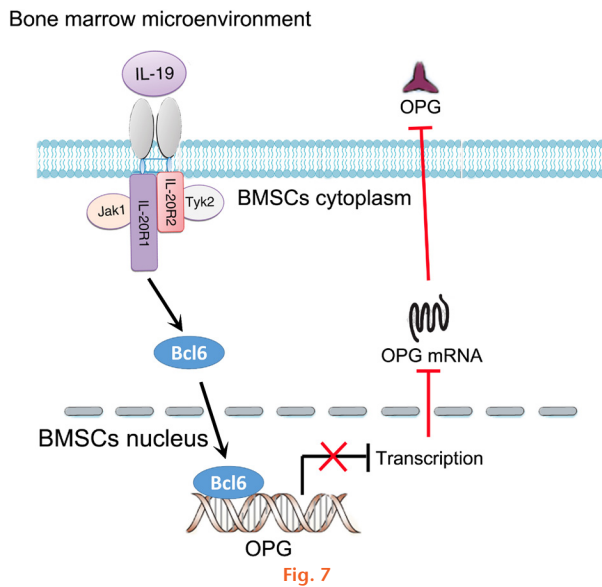


Diagram for the involvement of *interleukin (IL)-19* in lipopolysaccharide (LPS)-induced bone loss. LPS induces trabecular bone loss, in which *IL-19* levels are elevated significantly in response to LPS in peripheral blood serum and bone marrow. In bone marrow, *IL-19* binds to receptor on the cell membrane of bone mesenchymal stem cells (BMSCs) to suppress osteoprotegerin (OPG) transcription through Bcl6. OPG hypoproduction from BMSCs facilitates receptor activator of nuclear factor- κ B ligand (RANKL)-induced osteoclastic differentiation of bone marrow monocytes, which results in bone resorption activity enhancement and trabecular bone loss.

treatment (Supplementary Figure bb), suggesting that the promotion of osteoclast differentiation by *IL-19* is not achieved through direct effects.

The RANKL/OPG axis is critical for regulating bone resorption.²³ We examined the content of RANKL, OPG, and osteocalcin in peripheral blood and bone marrow from mice with LPS-induced bone loss (Supplementary Table iv). In the LPS-induced bone loss model, the content of RANKL and osteocalcin in serum (Figure 4a, Supplementary Figure ca) and the content of RANKL in femoral bone marrow suspension (Figure 4b) did not change significantly, but the content of OPG was significantly reduced compared with control mice (Figures 4c and 4d). Furthermore, global *IL-19* deletion had no significant effect on RANKL content in the serum (Figure 4e) and bone marrow (Figure 4f), but could increase the content of OPG in serum (Figure 4g) and femoral bone marrow (Figure 4h).

BMSCs and osteocytes were isolated from the bone marrow. Quantitative real-time polymerase chain reaction (RT-qPCR) results showed that the OPG mRNA of BMSCs in the LPS-treated group was decreased (Figure 5a), while OPG mRNA level of BMSCs in *IL-19*^{-/-} mice was increased (Figure 5b). However, OPG mRNA level in osteocytes of the LPS-treated mice was slightly increased, and there was no significant change in OPG mRNA levels in osteocytes of *IL-19*^{-/-} mice (Supplementary Figures cb and cc). To further verify whether *IL-19* directly regulates OPG production, primary BMSCs were treated with recombinant *IL-19* in vitro and the content

of OPG mRNA was significantly decreased (Figure 5c). However, recombinant *IL-19* treatment of primary osteocytes and MLO-Y4 osteocyte cell line showed no significant effect on OPG mRNA and protein secretion levels (Supplementary Figures cd and ce). Since *IL-19* mediates its function mainly by binding to the IL-20 receptor complex,²⁴ the membrane receptor IL-20R1 was downregulated by siRNA (Figure 5d). The results show that recombinant *IL-19* can significantly suppress OPG expression in BMSCs, but receptor IL-20R1 inhibition can reverse the function of *IL-19* (Figure 5e). The above results indicate that the inhibitory effect on OPG production in BMSCs by *IL-19* occurs via the IL-20R1 receptor to a large extent, if not completely.

***IL-19* suppresses OPG expression via Bcl6 in BMSCs.** To investigate the molecular mechanisms by which *IL-19* suppresses OPG expression in a LPS-induced bone loss mouse model, the proximal promoter of the mouse OPG gene was analyzed and revealed a transcriptional repressor Bcl6 binding site close to the transcription start site (Figure 6a). A luciferase reporter gene vector driven by the proximal promoter of OPG was constructed. The results of transient transfection experiments showed that deletion of the Bcl6 binding site can significantly increase luciferase activity (Figure 6b). Overexpression of Bcl6 by plasmid can significantly reduce the activity of the luciferase vector driven by the OPG promoter (Figure 6c), which proves that the Bcl6 binding site plays a negative role in the transcription of OPG. To further identify molecules binding on OPG promoter in BMSCs in response to recombinant *IL-19* treatment, ChIP experiments were performed, and the results demonstrated that *IL-19* promotes the binding of Bcl6 to the proximal promoter of OPG, and reduces the binding of RNAP II to this region. Furthermore, *IL-19* enhances the binding of Bcl6 to the OPG promoter and weakens the binding of RNAP II to this region, through interaction with the cell membrane receptor IL-20R1 (Figures 6d and 6e). When Bcl6 was downregulated by siRNA (Figure 6f), the experiments showed that Bcl6 mediated the inhibitory effect of *IL-19* on OPG (Figure 6g).

Discussion

As a common bone metabolic disease, primary osteoporosis is a systemic and metabolic disease characterized by progressive bone loss, degeneration of bone microstructure, and increased fragility fractures. Immune system malfunction has an important role in the development of primary osteoporosis, while inflammation is a direct contributor to osteoporosis. Various inflammatory markers, such as IL-1, IL-6, IL-17, and TNF- α , may upregulate RANKL expression in joints of patients with rheumatoid arthritis,²⁵⁻²⁷ which in turn induces osteoclastogenesis. Combined deficiency of IL-1/IL-6 has been reported to markedly ameliorate TNF-mediated arthritis and bilateral sacroiliitis.²⁸ In the elderly, circulating levels of IL-6 have been positively correlated with CRP and negatively correlated with BMD.²⁹ Previous studies have

shown that administration of moderate amounts of LPS by injection or nebulized inhalation to mice induces significant bone loss in a short period of time. The mechanism of bone loss is that LPS activates the RANKL pathway and promotes osteoclast proliferation and differentiation,³⁰ and also stimulates granulocyte colony-stimulating factor (G-CSF),^{31,32} which induces bone resorption. It also decreases the expression of Connexin 43 protein in osteoblasts and increases it in osteoclasts, and Connexin 43 gene deficiency reduces bone mass and inhibits bone formation in mice.^{33,34} Some studies suggest that treatment for chronic inflammation may be an adjunctive therapy for osteoporosis and ankylosing spondylitis.^{35,36} The relationship between *IL-19*, also an inflammatory factor, and osteoporosis has been less studied. In our present study, we focused on investigating the relationship between *IL-19* and bone mass, and investigated the potential mechanisms.

We demonstrated that *IL-19* levels were significantly elevated in peripheral blood serum and femoral bone marrow suspension in a LPS-induced bone loss mouse model, and level of *IL-19* in serum was negatively correlated with L1 vertebral body,^{37,38} and distal femoral BV/TV.³⁹ Previous research has shown that some cytokines, such as chemokine (C-C matrix) ligand 2 (CCL2), CCL3, CCL4, TNF- α , and IL-12p70, were significantly decreased in LPS-treated BALB/c *IL-19*^{-/-}, suggesting that *IL-19* may enhance the LPS response in BALB/c mice.⁴⁰ However, there are currently no results of similar experiments using C57BL/6 mice.⁴⁰ We used LPS to treat *IL-19*^{-/-} and WT C57BL/6 mice in this experiment, which led to increased BV/TV and Tb.N, and decreased Tb.Sp.³⁶

Moreover, global *IL-19* deletion had no effect on bone formation, but suppressed osteoclastogenesis in the LPS-treated mice group. Nevertheless, we did not detect the cytokines associated with C57BL/6 mice,⁴¹ and it remains to be further explored whether there is a decrease in cytokines such as CCL3, TNF- α , and CCL4 similar to that in BALB/c mice.

Several studies have shown that inflammatory factors including TNF- α , IL-1, IL-6, IL-17, and IL-22 are closely associated with bone remodelling, and that these activate BMSCs.^{42–46} BMSCs are multipotent stromal cells that differentiate into osteoblasts, which can secrete M-CSF, RANKL, and OPG to regulate osteoclast differentiation.⁴⁷ Osteoclasts and osteoblasts play an important role in bone remodelling, but the balance between them is disrupted during the development of osteoporosis. In our study, BMSCs were isolated from C57BL/6 mice,⁴⁸ and cultured with *IL-19* combined with M-CSF, as well as RANKL, to generate osteoclasts. TRAP staining showed no significant effect of *IL-19* on osteoclast differentiation, indicating that *IL-19* does not directly regulate this. In vitro experiments have shown that *IL-19* inhibits osteoblast differentiation by suppressing NF- κ B and 38 kD mitogen-activated protein kinases (p38MAPK) activation, as well as c-Fos expression, in the mouse macrophage-like cell line RAW264.7.^{41,49} We examined the levels of RANKL and OPG in peripheral blood and bone marrow of two groups of mice. In the LPS-induced bone loss mouse model, there was no significant change in RANKL content in serum and femoral

bone marrow suspension, but OPG content was significantly reduced. *IL-19* deficiency had no significant effect on RANKL content but increased OPG content in serum and femoral bone marrow, indicating that *IL-19* mainly affects OPG expression. To verify whether *IL-19* directly regulates OPG production, we treated primary BMSCs with recombinant *IL-19* in vitro to significantly decrease OPG mRNA content, while recombinant *IL-19* treatment of primary osteocytes and MLO-Y4 osteocyte, OPG mRNA, and protein secretion levels were not significantly affected, showing that the main target of *IL-19* in BMSCs was OPG, while recombinant *IL-19* significantly inhibited OPG expression in BMSCs. To further pursue the molecular mechanisms of *IL-19* inhibition of OPG expression in the LPS-induced bone loss mouse model, we identified a transcriptional repressor Bcl6 binding site near the transcriptional start site and constructed a luciferase reporter gene vector driven by the OPG proximal promoter. The results of transient transfection experiments showed that the Bcl6 binding site plays a negative role in the transcriptional regulation of the OPG gene. When Bcl6 was downregulated, Bcl6 mediated the repressive effect of *IL-19* on OPG (Figure 7).

Although our work suggests that *IL-19* can increase bone resorption, its role in the pathogenesis of osteoporosis is not fully understood. Its local and systemic actions are intricate and depend on a variety of complex factors, such as the involvement of differential receptors, the cell types involved, and their interactions. Therefore, targeting these endogenous mediators in osteoporosis remains challenging. The present research mainly clarifies that *IL-19* promotes bone resorption in the LPS-induced bone loss model in mice by inhibiting OPG expression, and that this inhibition may be related to the presence of a transcriptional repressor Bcl6 binding site near the OPG transcriptional start site. The results of this study should help to improve the current understanding of the mechanisms of inflammatory factors on bone loss and enable targeting of *IL-19* as a direction for targeted regulation of bone loss-related diseases. Since age is an important factor contributing to the activation of the inflammatory response and is strongly associated with osteoporosis, future studies are needed to determine whether ageing-induced osteoporosis is associated with changes in *IL-19* expression.

Supplementary material



Tables detailing the numerical data of the experimental results, and supplementary figures illustrating the response of bone marrow-derived monocytes to interleukin-19 (IL-19) treatment during osteoclast differentiation in vitro, as well as the effects of IL-19 on osteocalcin levels and osteoprotegerin expression in osteocytes. An ARRIVE checklist is also included to show that the ARRIVE guidelines were adhered to in this study.

References

- Liu YD, Liu JF, Liu B. N,N-Dimethylformamide inhibits high glucose-induced osteoporosis via attenuating MAPK and NF- κ B signalling. *Bone Joint Res.* 2022;11(4):200–209.
- Kim MH, Choi LY, Chung JY, Kim E-J, Yang WM. Auraptene ameliorates osteoporosis by inhibiting RANKL/NFATc1 pathway-mediated bone resorption based on network pharmacology and experimental evaluation. *Bone Joint Res.* 2022;11(5):304–316.
- Zhang Y, Yan M, Yu Q-F, et al. Puerarin prevents LPS-induced osteoclast formation and bone loss via inhibition of Akt activation. *Biol Pharm Bull.* 2016;39(12):2028–2035.
- Azuma Y, Kaji K, Katogi R, Takeshita S, Kudo A. Tumor necrosis factor- α induces differentiation of and bone resorption by osteoclasts. *J Biol Chem.* 2000;275(7):4858–4864.
- Yamaguchi R, Yoshimura A, Yoshioka H, Kaneko T, Hara Y. Ability of supragingival plaque to induce toll-like receptor 4-mediated stimulation is associated with cytokine production by peripheral blood mononuclear cells. *J Periodontol.* 2009;80(3):512–520.
- Watanabe K, Iizuka T, Adeleke A, et al. Involvement of toll-like receptor 4 in alveolar bone loss and glucose homeostasis in experimental periodontitis. *J Periodontol Res.* 2011;46(1):21–30.
- Li J, Ho WTP, Liu C, et al. The role of gut microbiota in bone homeostasis. *Bone Joint Res.* 2021;10(1):51–59.
- AlQranei MS, Senbanjo LT, Aljohani H, Hamza T, Chellaiah MA. Lipopolysaccharide- TLR-4 Axis regulates osteoclastogenesis independent of RANKL/ RANK signaling. *BMC Immunol.* 2021;22(1):23.
- Sultana S, Dey R, Bishayi B. Dual neutralization of TNFR-2 and MMP-2 regulates the severity of *S. aureus* induced septic arthritis correlating alteration in the level of interferon gamma and interleukin-10 in terms of TNFR2 blocking. *Immunol Res.* 2018;66(1):97–119.
- Zhang Y, Jiang B, Zhang P, Chiu SK, Lee MH. Complete abrogation of key osteoclast markers with a membrane-anchored tissue inhibitor of metalloproteinase: a novel approach in the prevention of osteoclastogenesis. *Bone Joint Res.* 2022;11(11):763–776.
- Lin L, Guo Z, He E, et al. SIRT2 regulates extracellular vesicle-mediated liver-bone communication. *Nat Metab.* 2023;5(5):821–841.
- Schilling AF, Filke S, Lange T, et al. Gap junctional communication in human osteoclasts in vitro and in vivo. *J Cell Mol Med.* 2008;12(6A):2497–2504.
- Fan G, Jiang X, Wu X, et al. Anti-inflammatory activity of tanshinone IIA in LPS-stimulated RAW264.7 macrophages via miRNAs and TLR4-NF- κ B pathway. *Inflammation.* 2016;39(1):375–384.
- Chen J, Caspi RR, Chong WP. IL-20 receptor cytokines in autoimmune diseases. *J Leukoc Biol.* 2018;104(5):953–959.
- Kragstrup TW, Andersen T, Heftdal LD, et al. The IL-20 cytokine family in rheumatoid arthritis and spondyloarthritis. *Front Immunol.* 2018;9:2226.
- Azuma Y-T, Nakajima H, Takeuchi T. IL-19 as a potential therapeutic in autoimmune and inflammatory diseases. *Curr Pharm Des.* 2011;17(34):3776–3780.
- Leng R-X, Pan H-F, Tao J-H, Ye D-Q. IL-19, IL-20 and IL-24: potential therapeutic targets for autoimmune diseases. *Expert Opin Ther Targets.* 2011;15(2):119–126.
- Niess JH, Hruz P, Kaymak T. The interleukin-20 cytokines in intestinal diseases. *Front Immunol.* 2018;9:1373.
- Robling AG, Bonewald LF. The osteocyte: New insights. *Annu Rev Physiol.* 2020;82:485–506.
- Sharaf-Eldin WE, Abu-Shahba N, Mahmoud M, El-Badri N. The modulatory effects of mesenchymal stem cells on osteoclastogenesis. *Stem Cells Int.* 2016;2016:1908365.
- Han Y, You X, Xing W, Zhang Z, Zou W. Paracrine and endocrine actions of bone-tissue functions of secretory proteins from osteoblasts, osteocytes, and osteoclasts. *Bone Res.* 2018;6:16.
- Chow DH, Zheng L, Tian L, Ho KS, Qin L, Guo X. Application of ultrasound accelerates the decalcification process of bone matrix without affecting histological and immunohistochemical analysis. *J Orthop Translat.* 2019;17:112–120.
- Hooshiar SH, Tobeiha M, Jafarnejad S. Soy isoflavones and bone health: Focus on the RANKL/RANK/OPG pathway. *Biomed Res Int.* 2022;2022:8862278.
- Liu S, Flores JJ, Li B, et al. IL-20R activation via rIL-19 enhances hematoma resolution through the IL-20R1/ERK/Nrf2 pathway in an experimental GMH rat pup model. *Oxid Med Cell Longev.* 2021;2021:5913424.
- Takeuchi T, Yoshida H, Tanaka S. Role of interleukin-6 in bone destruction and bone repair in rheumatoid arthritis. *Autoimmun Rev.* 2021;20(9):102884.
- Taams LS. Interleukin-17 in rheumatoid arthritis: Trials and tribulations. *J Exp Med.* 2020;217(3):e20192048.
- Di Muzio C, Cipriani P, Ruscitti P. Rheumatoid arthritis treatment options and type 2 diabetes: Unravelling the association. *BioDrugs.* 2022;36(6):673–685.
- Hayer S, Niederreiter B, Kalkgruber M, et al. Analysis of combined deficiency of interleukin-1 and -6 versus single deficiencies in TNF-mediated arthritis and systemic bone loss. *Bone Joint Res.* 2022;11(7):484–493.
- Ding C, Parameswaran V, Udayan R, Burgess J, Jones G. Circulating levels of inflammatory markers predict change in bone mineral density and resorption in older adults: A longitudinal study. *J Clin Endocrinol Metab.* 2008;93(5):1952–1958.
- Sul OJ, Park HJ, Son HJ, Choi HS. Lipopolysaccharide (LPS)-induced autophagy is responsible for enhanced osteoclastogenesis. *Mol Cells.* 2017;40(11):880–887.
- Dekkers PE, Juffermans NP, Hove Tt, de Jonge E, van Deventer SJ, van Der Poll T. Granulocyte colony-stimulating factor receptors on granulocytes are down-regulated after endotoxin administration to healthy humans. *J Infect Dis.* 2000;181(6):2067–2070.
- Boettcher S, Gerosa RC, Radpour R, et al. Endothelial cells translate pathogen signals into G-CSF-driven emergency granulopoiesis. *Blood.* 2014;124(9):1393–1403.
- Bivi N, Nelson MT, Faillace ME, Li J, Miller LM, Plotkin LI. Deletion of Cx43 from osteocytes results in defective bone material properties but does not decrease extrinsic strength in cortical bone. *Calcif Tissue Int.* 2012;91(3):215–224.
- Li G, Zhang L, Lu Z, et al. Connexin 43 channels in osteocytes are necessary for bone mass and skeletal muscle function in aged male mice. *Int J Mol Sci.* 2022;23(21):13506.
- Livshits G, Kalinkovich A. Targeting chronic inflammation as a potential adjuvant therapy for osteoporosis. *Life Sci.* 2022;306:120847.
- Liao H-T, Tsai C-Y. Cytokines and regulatory T cells in ankylosing spondylitis. *Bone Joint Res.* 2023;12(2):133–137.
- Cheng B, Wen Y, Yang X, et al. Gut microbiota is associated with bone mineral density: an observational and genome-wide environmental interaction analysis in the UK Biobank cohort. *Bone Joint Res.* 2021;10(11):734–741.
- Bukowski BR, Sandhu KP, Bernatz JT, et al. CT required to perform robotic-assisted total hip arthroplasty can identify previously undiagnosed osteoporosis and guide femoral fixation strategy. *Bone Joint J.* 2023;105-B(3):254–260.
- Zhou M-S, Tao Z-S. Systemic administration with melatonin in the daytime has a better effect on promoting osseointegration of titanium rods in ovariectomized rats. *Bone Joint Res.* 2022;11(11):751–762.
- Azuma Y-T, Nishiyama K. Interleukin-19 enhances cytokine production induced by lipopolysaccharide and inhibits cytokine production induced by polyI:C in BALB/C mice. *J Vet Med Sci.* 2020;82(7):891–896.
- Jia Y, Qi X, Ma M, et al. Integrating genome-wide association study with regulatory SNP annotations identified novel candidate genes for osteoporosis. *Bone Joint Res.* 2023;12(2):147–154.
- Medhat D, Rodríguez CI, Infante A. Immunomodulatory effects of MSCs in bone healing. *Int J Mol Sci.* 2019;20(21):5467.
- Lieder R, Sigurjonsson OE. The effect of recombinant human interleukin-6 on osteogenic differentiation and YKL-40 expression in human, bone marrow-derived mesenchymal stem cells. *Biores Open Access.* 2014;3(1):29–34.
- Ma L, Aijima R, Hoshino Y, et al. Transplantation of mesenchymal stem cells ameliorates secondary osteoporosis through interleukin-17-impaired functions of recipient bone marrow mesenchymal stem cells in MRL/lpr mice. *Stem Cell Res Ther.* 2015;6(1):104.
- El-Zayadi AA, Jones EA, Churchman SM, et al. Interleukin-22 drives the proliferation, migration and osteogenic differentiation of mesenchymal stem cells: a novel cytokine that could contribute to new bone formation in spondyloarthropathies. *Rheumatology (Oxford).* 2017;56(3):488–493.
- Liu H, Xu GW, Wang YF, et al. Composite scaffolds of nano-hydroxyapatite and silk fibroin enhance mesenchymal stem cell-based bone regeneration via the interleukin 1 α autocrine/paracrine signaling loop. *Biomaterials.* 2015;49:103–112.
- Ma Q-L, Fang L, Jiang N, et al. Bone mesenchymal stem cell secretion of sRANKL/OPG/M-CSF in response to macrophage-mediated inflammatory response influences osteogenesis on nanostructured Ti surfaces. *Biomaterials.* 2018;154:234–247.
- Chen X, Chen W, Aung ZM, Han W, Zhang Y, Chai G. LY3023414 inhibits both osteogenesis and osteoclastogenesis through the PI3K/Akt/GSK3 signalling pathway. *Bone Joint Res.* 2021;10(4):237–249.
- Tsubaki M, Takeda T, Matsuda T, et al. Interleukin 19 suppresses RANKL-induced osteoclastogenesis via the inhibition of NF- κ B and p38MAPK activation and c-Fos expression in RAW264.7 cells. *Cytokine.* 2021;144:155591.

Author information:

- Z. Dai, MD, Graduate Student
- Y. Chen, MD, Graduate Student
- E. He, PhD, Graduate Student
- H. Wang, MD, Orthopaedic Surgeon
- W. Guo, MD, Orthopaedic Surgeon
- Q. Zhao, PhD, Orthopaedic Surgeon
Department of Orthopedics, Shanghai General Hospital, Shanghai Jiao Tong University School of Medicine, Shanghai, China.
- Z. Wu, PhD, Orthopaedic Surgeon, Department of Pediatric Orthopaedics, Shanghai Xinhua Hospital, Shanghai Jiao Tong University School of Medicine, Shanghai, China.
- K. Huang, PhD, Orthopaedic Surgeon, Department of Orthopedics, Zhabei Central Hospital of Jing'an District, Shanghai, China.

Author contributions:

- Z. Dai: Data curation, Formal analysis, Writing – original draft.
- Y. Chen: Data curation, Formal analysis.
- E. He: Formal analysis, Writing – original draft.
- H. Wang: Methodology, Software.
- W. Guo: Data curation, Software.
- Z. Wu: Writing – review & editing.
- K. Huang: Writing – review & editing.
- Q. Zhao: Funding acquisition, Supervision, Writing – review & editing.

Funding statement:

- The authors disclose receipt of the following financial or material support for the research, authorship, and/or publication of this article: funding from the Shanghai Natural Science Foundation (19ZR1440700); Medical-Industrial Interdisciplinary Research Fund of Shanghai Jiao Tong University (YG2017MS02); Youth Science and Technology Innovation Studio of Shanghai Jiao Tong University School of Medicine (JYKCGZS8); and Practice training base for interdisciplinary innovative talents of Shanghai Jiao Tong University (SJTUJXCX-3).

ICMJE COI statement:

- All authors report financial support for the study from: the Shanghai Natural Science Foundation (19ZR1440700); Medical-Industrial Interdisciplinary Research Fund of Shanghai Jiao Tong University (YG2017MS02); Youth Science and Technology Innovation Studio of Shanghai Jiao Tong University School of Medicine (JYKCGZS8); and Practice training base for interdisciplinary innovative talents of Shanghai Jiao Tong University (SJTUJXCX-3).

Data sharing:

- All data generated or analyzed during this study are included in the published article and/or in the supplementary material.

Acknowledgements:

- We would like to acknowledge the financial support we have received, and the outstanding animal facilities from Shanghai SLAC Laboratory Animal Co. Ltd.

Ethical review statement:

- The animal experiments were performed in accordance with the approved guidelines by the Institutional Animal Care and Use Committee affiliated with Shanghai General Hospital, Shanghai Jiao Tong University School of Medicine.

Open access funding:

- The authors report that they received open access funding for their manuscript from: Shanghai Natural Science Foundation (19ZR1440700); Medical-Industrial Interdisciplinary Research Fund of Shanghai Jiao Tong University (YG2017MS02); Youth Science and Technology Innovation Studio of Shanghai Jiao Tong University School of Medicine (JYKCGZS8); and Practice training base for interdisciplinary innovative talents of Shanghai Jiao Tong University (SJTUJXCX-3).

© 2023 Zhao et al. This is an open-access article distributed under the terms of the Creative Commons Attribution Non-Commercial No Derivatives (CC BY-NC-ND 4.0) licence, which permits the copying and redistribution of the work only, and provided the original author and source are credited. See <https://creativecommons.org/licenses/by-nc-nd/4.0/>